Temperature-Dependent Photoluminescence Imaging and Characterization of a Multi-Crystalline Silicon Solar Cell Defect Area

Preprint

Steve Johnston, Fei Yan, Jian Li,
Manuel J. Romero, and Mowafak Al-Jassim
National Renewable Energy Laboratory

Katherine Zaunbrecher
National Renewable Energy Laboratory and Colorado State University

Omar Sidelkheir and Alain Blosse
Calisolar

Presented at the 37th IEEE Photovoltaic Specialists Conference (PVSC 37)
Seattle, Washington
June 19-24, 2011

Conference Paper
NREL/CP-5200-50706
July 2011

Contract No. DE-AC36-08GO28308

NOTICE

Available electronically at http://www.osti.gov/bridge

Available for a processing fee to U.S. Department of Energy
and its contractors, in paper, from:

U.S. Department of Energy
Office of Scientific and Technical Information

P.O. Box 62
Oak Ridge, TN 37831-0062
phone: 865.576.8401
fax: 865.576.5728
email: mailto:reports@adonis.osti.gov

Available for sale to the public, in paper, from:

U.S. Department of Commerce
National Technical Information Service
5285 Port Royal Road
Springfield, VA 22161
phone: 800.553.6847
fax: 703.605.6900
email: orders@ntis.fedworld.gov
online ordering: http://www.ntis.gov/help/ordermethods.aspx

Cover Photos: (left to right) PIX 16416, PIX 17423, PIX 16560, PIX 17613, PIX 17436, PIX 17721

Printed on paper containing at least 50% wastepaper, including 10% post consumer waste.

TEMPERATURE-DEPENDENT PHOTOLUMINESCENCE IMAGING AND CHARACTERIZATION OF A MULTI-CRYSTALLINE SILICON SOLAR CELL DEFECT AREA

Steve Johnston[1], Fei Yan[1], Jian Li[1], Katherine Zaunbrecher[1,2], Manuel J. Romero[1], Mowafak Al-Jassim[1], Omar Sidelkheir[3], and Alain Blosse[3]
[1]National Renewable Energy Laboratory, Golden, CO, USA
[2]Colorado State University, Fort Collins, CO, USA
[3]Calisolar, Sunnyvale, CA, USA

ABSTRACT

Photoluminescence (PL) imaging is used to detect areas in multi-crystalline silicon that appear dark in band-to-band imaging due to high recombination. Steady-state PL intensity can be correlated to effective minority-carrier lifetime, and its temperature dependence can provide additional lifetime-limiting defect information. An area of high defect density has been laser cut from a multi-crystalline silicon solar cell. Both band-to-band and defect-band PL imaging have been collected as a function of temperature from ~85 to 350 K. Band-to-band luminescence is collected by an InGaAs camera using a 1200-nm short-pass filter, while defect band luminescence is collected using a 1350-nm long pass filter. The defect band luminescence is characterized by cathodo-luminescence. Small pieces from adjacent areas within the same wafer are measured by deep-level transient spectroscopy (DLTS). DLTS detects a minority-carrier electron trap level with an activation energy of 0.45 eV on the sample that contained defects as seen by imaging.

INTRODUCTION

Photoluminescence (PL) imaging of multi-crystalline silicon can quickly characterize wafers and cells to detect areas containing defects such as dense regions of grain boundaries and dislocation/defect clusters. [1-8] For band-to-band radiative recombination, defect areas are relatively dark due to non-radiative or sub-bandgap defect recombination. Some defects can be revealed and characterized directly by sub-bandgap radiative transitions. Silicon is known to have such sub-bandgap states with radiative emissions in the ~1250–1550 nm wavelength range. [9-12]

EXPERIMENT

Band-to-band PL and defect band emissions are imaged using a FLIR SC2500 InGaAs camera with sensitivity to detect photons with wavelengths from 0.9 to 1.7 μm. The camera contains a lock-in detection option to improve the signal-to-noise ratio. For defect band emission imaging, a long-pass filter with a cut-off wavelength at 1350 nm is used to block band-to-band PL. The light source is composed of four 810-nm laser diodes with engineered diffusers to spread out the light over the sample. The intensity is near that of one sun, or ~100 mW/cm^2. Defect band PL is collected when pulsing the 810-nm laser diode excitation at about 7 Hz. Figure 1 shows both band-to-band PL imaging (top) and defect band emission imaging (bottom) of part of a multi-crystalline silicon solar cell.

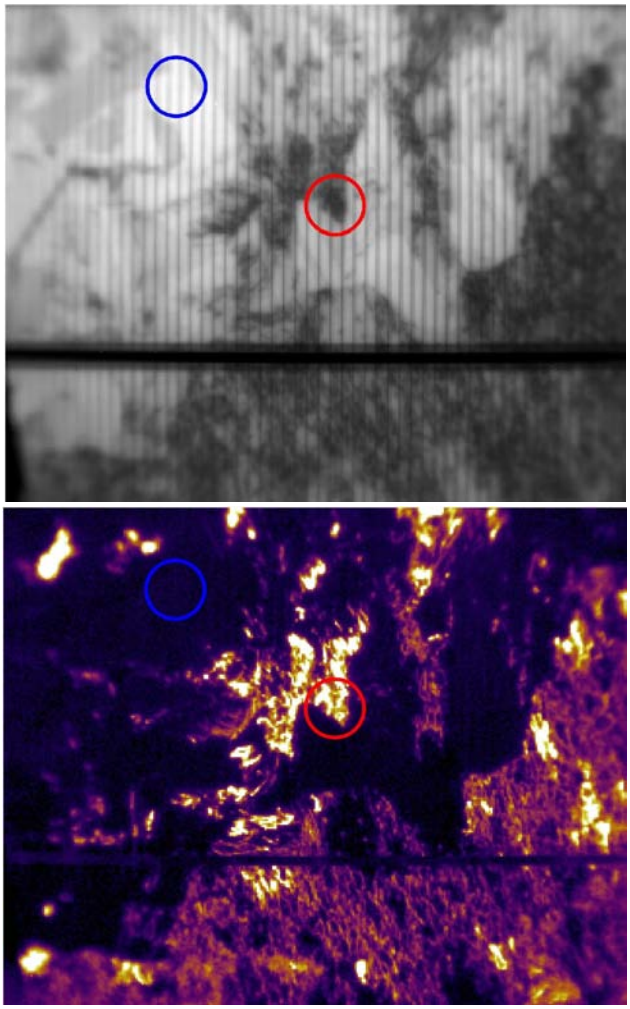

Figure 1 PL images of a portion of a finished multi-crystalline silicon solar cell showing band-to-band PL (top) and defect band emission (bottom). The red circled area contains a high-defect-density region, while the blue circle represents a relatively defect-free area.

In Fig. 1, the circled areas were cut out of the wafer using a Q-switched Nd:YAG pulsed laser doubled to 532 nm wavelength. Laser damage was smoothed by sanding the edges of the ~1-cm-diameter cut pieces. The blue area is intended to be a relatively defect-free area, while the red area contains a high-defect-density area. The bottom image shows sub-bandgap defect band luminescence when using a 1350-nm long-pass filter in addition to long-pass RG1000 Schott glass filters used to block reflected 810-nm laser diode light. The red circled area contains high emissions of the sub-bandgap luminescence. A plot of the current vs. voltage for these cut out pieces is shown in Fig. 2. The piece containing the defect area (red curve) shows diode breakdown in reverse bias at a reduced voltage compared to the piece from the relatively defect-free area (blue curve).

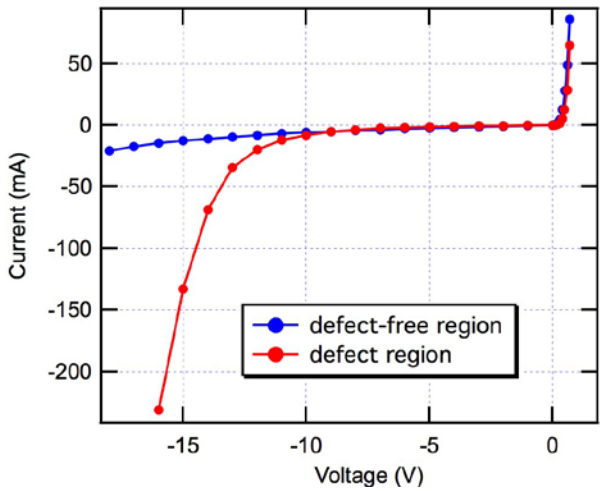

Figure 2 Current vs. voltage curves for the laser-cut regions. The red curve represents the piece containing the high-defect-density region, while the blue curve represents the relatively defect-free piece.

PL imaging of the high-defect-density red circle area of Fig.1 is shown in Fig. 3. Images at selected temperatures are shown for both band-to-band imaging (left column) and defect band imaging (right column). The sample was cooled in a cryostat using liquid nitrogen. A laser diode with an 810-nm wavelength and approximately one-sun intensity was used to illuminate the sample. The FLIR InGaAs camera was used to collect the images as temperature was varied. A relatively defect-free area is circled in blue on the lowest temperature band-to-band PL image. The average PL intensity within this area is plotted as a function of temperature and represented by the blue circle points in Fig. 4. The red outlined rectangular area of Fig. 3 represents a high-defect-density region, and this area is averaged and represented by the red square markers in the plots of Fig. 4. For the defect band images of Fig. 3, a green triangle roughly outlines the high-defect area. The average defect band intensity is also plotted in Fig. 4 using green triangle markers, which are referenced to the right axis.

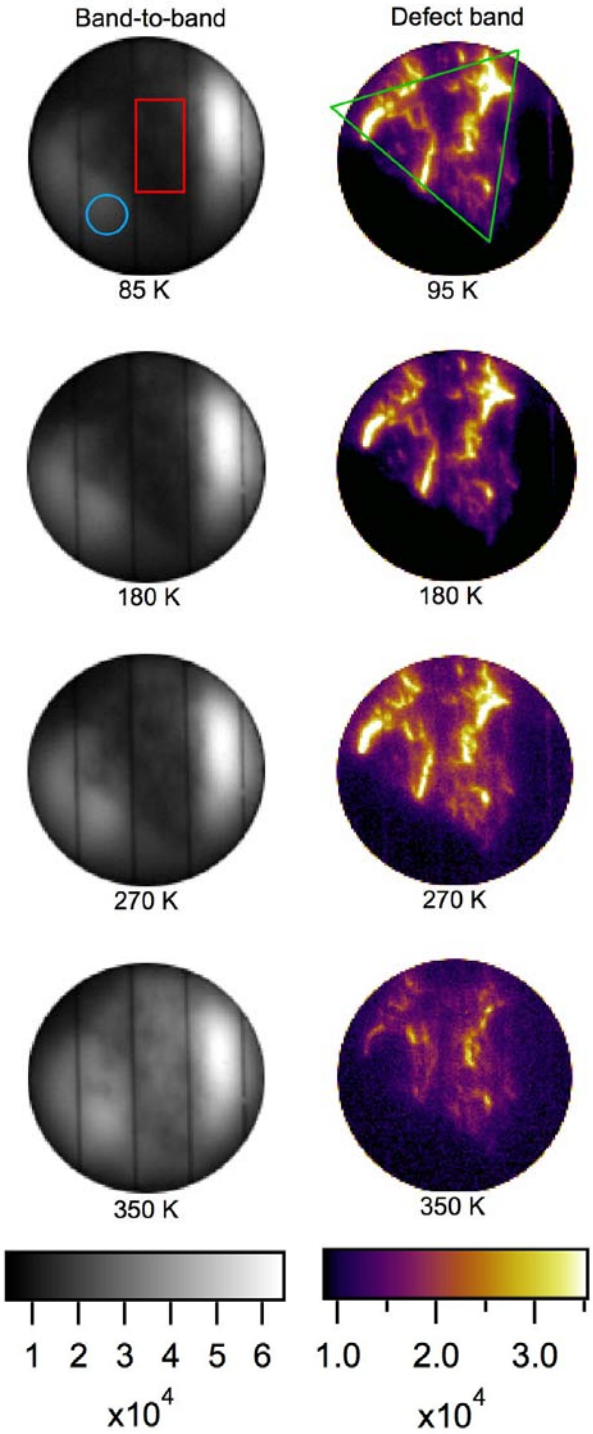

Figure 3 PL imaging at selected temperatures performed on the red cut-out piece from Fig 1. The left column shows band-to-band PL, while the right column shows sub-bandgap defect band emissions. The red outlined rectangular area contains high defect density, and the blue circular area represents a relatively defect-free area. The green triangle is used to define average defect band emissions.

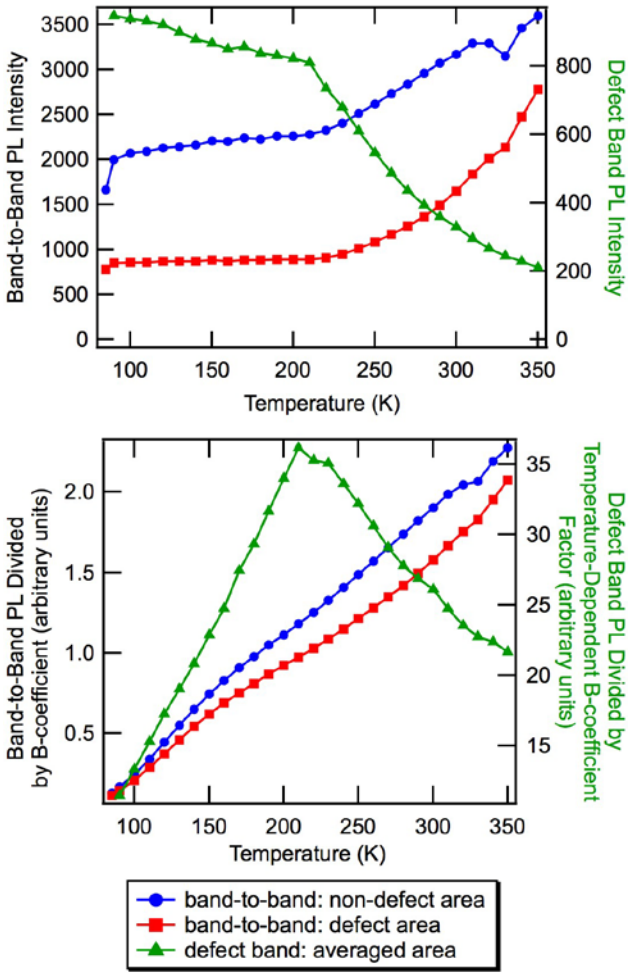

Figure 4 Average PL intensities (band-to-band on left axis and defect band on right axis) of the areas defined in Fig. 3 are plotted as a function of temperature (top). The band-to-band intensities are divided by the temperature-dependent B-coefficient for silicon in the bottom graph. The bottom plot also shows the defect band intensities divided by a temperature-dependent B-coefficient factor.

The band-to-band PL intensities for both the defect and defect-free areas are shown to increase with temperature in the top graph of Fig. 4. The defect band intensity, however, is shown to decrease with increasing temperature. The B-coefficient for radiative recombination in silicon has a known temperature dependence. [13,14] The average band-to-band PL intensity can account for this variation by dividing the PL values by the B-coefficient. The results are plotted on the bottom graph of Fig. 4. There is now a near-linear increase in band-to-band PL with temperature. This trend is due to the temperature dependence of the minority-carrier lifetime, as shown in Fig. 5. Minority-carrier lifetime has been measured on this cut-out area of the finished cell by the open-circuit voltage decay technique. [15,16] When compared over the same temperature range, the factor of increase in the average PL intensity is comparable to the factor of increase in lifetime, such that dividing PL intensity by lifetime yields a roughly flat, temperature-independent set of values.

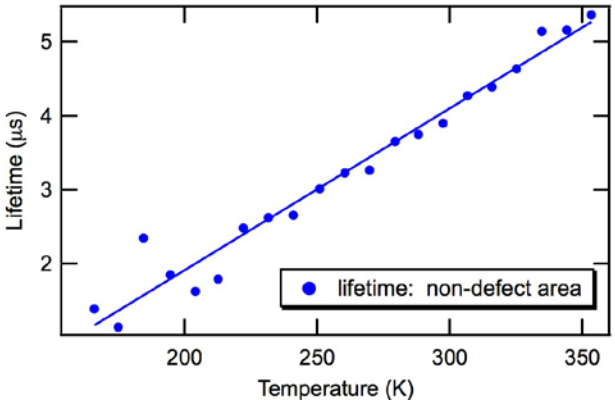

Figure 5 Temperature-dependent minority-carrier lifetime of the blue-circled area of Fig. 1 as measured by open-circuit voltage decay.

As shown in Fig. 4, the defect band points are divided by an equivalent B-coefficient factor based on temperature-dependent bandgap [17,18], whose values similarly decrease with temperature like those of the band-to-band PL B-coefficient. The defect band PL intensity data shows a change in slope at approximately 210 K (top graph in Fig. 4). The temperature-dependent, bandgap-based corrected data then shows a peak at this value (bottom graph of Fig. 4), which suggests a defect signature.

To further characterize the band-to-band PL and defect band emissions, we have performed cathodo-luminescence (CL) mapping to collect high-resolution spatial and spectral data. CL was measured on a roughly 200 μm x 200 μm defect-containing area from the red circled piece of Fig. 1. The sample is cooled to approximately 78 K. Figure 6 shows the CL mapping results for band-to-band transitions near 1130 nm (top image) and for defect band transitions near 1400 nm (lower image). The top image shows a dark line representing a grain boundary or dislocation where recombination through impurity and/or defect states is high. In the lower image, this same dark feature is evident, and sub-bandgap emissions are revealed very near to this line. Spectral data is gathered at three points in the vicinity of this defect area. The first point, p1 (shown in blue), represents an area where defect band emissions are very weak. The corresponding spectrum shown in the bottom graph of Fig. 6 shows a peak centered at ~1100 nm for the band-to-band radiative transition but no sub-bandgap signal. The other points, p2 and p3 (shown in red and orange in Fig. 6), correspond to areas where defect band emission is relatively high. The spectrums corresponding to these spots show peaks of defect band emissions in the 1300–1600 nm range.

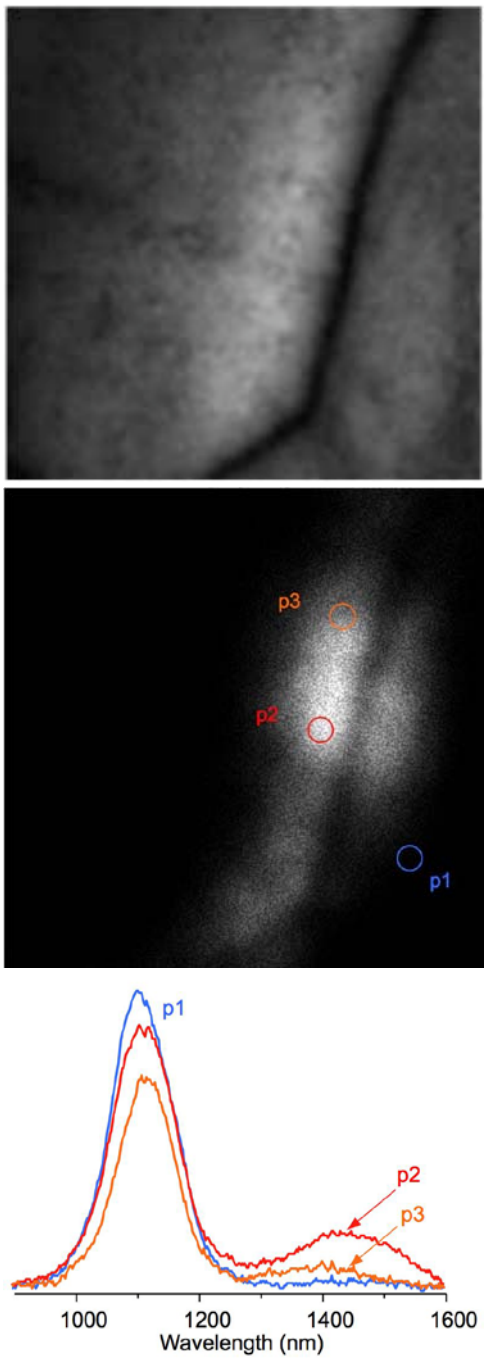

Figure 6 Cathodoluminescence mapping is performed on a roughly 200 μm x 200 μm defect-containing area from the red circled piece of Fig. 1. The top image shows intensities at ~1130 nm, while the lower image represents defect band intensities with wavelengths in the 1300–1600 nm range. The bottom graph shows spectrums from the points labeled in the defect band image.

A small, roughly 1 mm x 2 mm sample was cleaved from a nearby defect region for deep-level transient spectroscopy (DLTS). A sample of this size or smaller is required for DLTS due to limitations on the value of capacitance for this measurement. Figure 7 shows band-to-band electroluminescence imaging [19,20] (top) and defect band emissions (bottom) when a forward bias is applied to this sample. This piece shows similar defect structures to the neighboring piece used for temperature-dependent imaging.

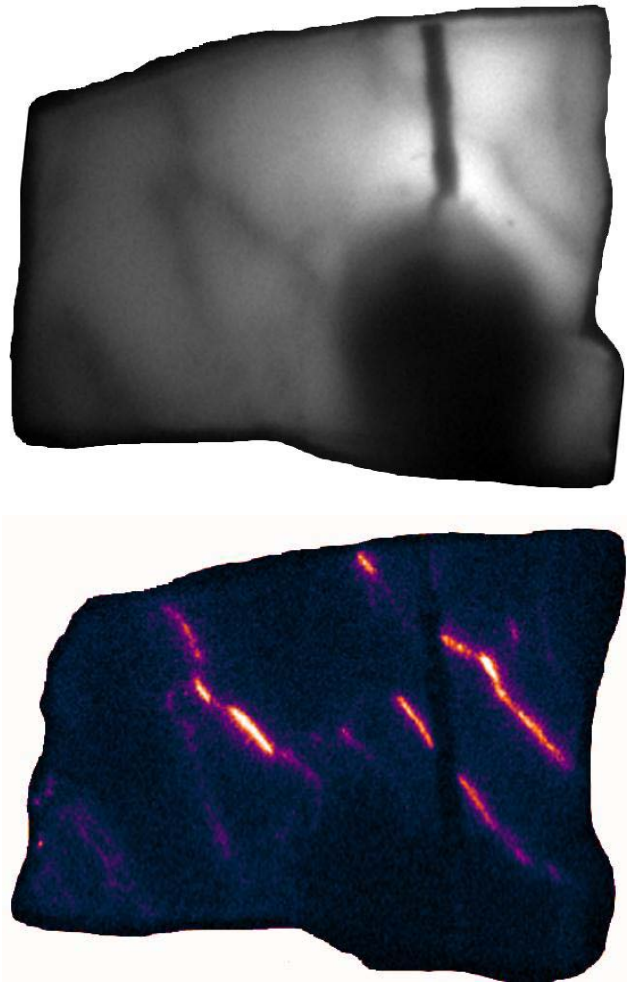

Figure 7 Electroluminescence images acquired with forward bias show band-to-band emissions in the top image and defect band emission in the bottom image. The top image is partially obscured due to the large probe pin contacting the grid line.

DLTS data was collected using a reverse bias of 5 V and filling pulses to 0.2 V forward bias. A positive peak, corresponding to a minority-carrier electron trap, was evident. Analysis of the DLTS data is used to generate the Arrhenius plot shown in Fig. 8., where the DLTS-detected peak corresponds to a defect level with an activation energy of 0.45 eV. A similarly prepared and sized sample from a defect-free area did not show a discernible peak when also measured by DLTS.

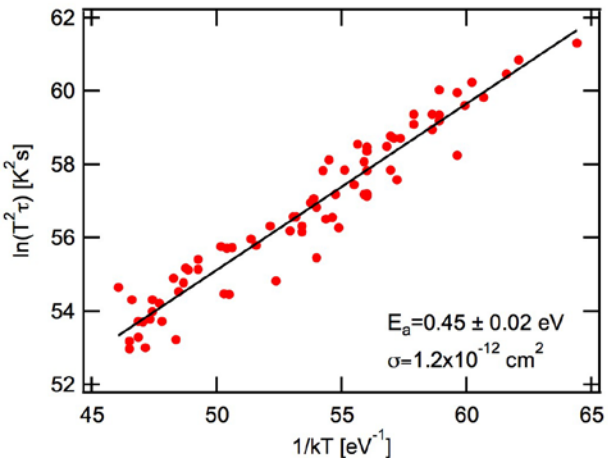

Figure 8 DLTS data from the sample shown in Fig. 7 is analyzed to construct an Arrhenius plot. The slope corresponds to an activation energy of 0.45 eV, while the intercept relates to a capture cross section of 1.2×10^{-12} cm^2.

SUMMARY

Temperature-dependent PL imaging was collected on samples from a multi-crystalline silicon solar cell. A defect-containing region was compared to a relatively defect-free region using both band-to-band PL and defect band emissions. The temperature dependence of the band-to-band PL is due to the temperature variations of the B-coefficient for radiative recombination and minority carrier lifetime. The temperature dependence of the defect band emissions shows a potential defect signature. CL mapping showed the defect band spectrum had a peak in the 1300–1600 nm range. DLTS was used to measure a minority-carrier electron trap with an activation energy of 0.45 eV on a defect-containing sample.

ACKNOWLEDGEMENT

This work was supported by the U.S. Department of Energy under Contract No. DE-AC36-08GO28308 with the National Renewable Energy Laboratory and with support from the American Recovery and Reinvestment Act.

REFERENCES

[1] T. Trupke, R. A. Bardos, M. C. Schubert, and W. Warta, "Photoluminescence Imaging of Silicon Wafers", *Appl. Phys. Lett.* **89**, 2006, 044107.

[2] T. Trupke, R. A. Bardos, M. D. Abbott, F. W. Chen, J. E. Cotter, and A. Lorenz, "Fast Photoluminescence Imaging of Silicon Wafers", *32nd IEEE PVSC* and *WCPEC-4*, 2006, pp. 928-931.

[3] W. McMillan, T. Trupke, J. W. Weber, M. Wagner, U. Mareck, Y. C. Chou, and J. Wong, "In-line Monitoring of Electrical Wafer Quality Using Photoluminescence Imaging", 25th EPVSEC/5th WCPEC, Valencia, Spain, 2010, pp. 1346-1351.

[4] J. Haunschild, M. Glatthaar, M. Demant, J. Nievendick, M. Motzko, S. Rein, and E. R. Weber, "Quality control of as-cut multicrystalline silicon wafers using photoluminescence imaging for solar cell production", Sol. Ener. Mat. & Sol. Cells 94, 2010, pp. 2007-2012.

[5] T. Trupke, J. Nyhus, and J. Haunschild, "Luminescence imaging for inline characterization in silicon photovoltaics", Phys. Status Solidi RRL **5**, 2011, pp. 131-137.

[6] T. Trupke, J. Nyhus, R. A. Sinton, and J. W. Weber, "Photoluminescence imaging on silicon bricks", Proceedings of the 24th European Photovoltaic Solar Energy Conference, Hamburg, Germany, 2009, pp. 1029-1033.

[7] B. Mitchell, T. Trupke, J. W. Weber, and J. Nyhus, "Bulk minority carrier lifetimes and doping of silicon bricks from photoluminescence intensity ratios", J. Appl. Phys. **109**, 2011, 083111.

[8] J. Haunschild, M. Glatthaar, S. Riepe, and S. Rein, "Quality control using luminescence imaging in production of mc-silicon solar cells from UMG feedstock", 35th IEEE PVSC, 2010, pp. 812-816.

[9] I. Tarasov, S. Ostapenko, C. Haessler, and E. U. Reisner, "Spatially resolved defect diagnostics in multicrystalline silicon for solar cells," Mat. Sci. & Engr. B **71** (1-3), 51-55 (2000).

[10] S. Ostapenko, I. Tarasov, J. P. Kalejs, C. Haessler, and E.-U. Reisner, "Defect monitoring using scanning photoluminescence spectroscopy in multicrystalline silicon wafers", Semicond. Sci. Technol. **15**, 2000, pp. 840-848.

[11] I. Tarasov, S. Ostapenko, W. Seifert, M. Kittler, J. P. Kaleis, "Defect diagnostics in multicrystalline silicon using scanning techniques", Physica B **308-310**, 2001, pp. 1133-1136.

[12] M. Kittler, W. Seifert, T. Arguirov, I. Tarasov, and S. Ostapenko, "Room-temperature luminescence and electron-beam-induced current (EBIC) recombination behaviour of crystal defects in multicrystalline silicon", Sol. Ener. Mat. & Sol. Cells **72**, 2002, pp. 465-472.

[13] H. Schlangenotto, H. Maeder, and W. Gerlach, "Temperature Dependence of the Radiative Recombination Coefficient in Silicon", Phys. Stat. Sol. (a) **21**, 1974, pp. 357-367.

[14] T. Trupke, M. A. Green, P. Wurfel, P. P. Altermatt, A. Wang, J. Zhao, and R. Corkish, "Temperature dependence of the radiative recombination coefficient of intrinsic crystalline silicon", J. Appl. Phys. **94**, 2003, pp. 4930-4937.

[15] B. R. Gossick, “Post-Injection Barrier Electromotive Force of p-n Junctions”, Phys. Rev. **91**, 1953, pp. 1012-1013.

[16] S. R. Lederhandler and L. J. Giacoletto, “Measurement of Minority Carrier Lifetime and Surface Effects in Junction Devices”, Proceedings of the IRE **43**, 1955, pp. 477-483.

[17] W. Bludau, A. Onton, and W. Heinke, “Temperature dependence of the band gap of silicon”, J. Appl. Phys. **45**, 1974, pp. 1846-1848.

[18] D. Z. Garbuzov, “Reradiation effects, lifetimes and probabilities of band-to-band transitions in direct A_3B_5 compounds of GaAs type”, Journal of Luminescence **27**, 1982, pp. 109-112.

[19] T. Fuyuki, H. Kondo, T. Yamazaki, Y. Takahashi, and Y. Uraoka, “Photographic Surveying of Minority Carrier Diffusion Length in Polycrystalline Silicon Solar Cells by Electroluminescence”, *Appl. Phys. Lett.* **86**, 2005, 262108.

[20] T. Fuyuki, H. Kondo, Y. Kaji, A. Ogane, and Y Takahashi, “Analytic Findings in the Electroluminescence Characterization of Crystalline Silicon Solar Cells”, *J. Appl. Phys.* **101**, 2007, 023711.